Iron solubility in fine particles associated with secondary acidic aerosols in east China

Zhu, Yanhong; Li, Weijun; Lin, Qiuhan; Yuan, Qi; Liu, Lei; Zhang, Jian; Zhang, Yinxiao; Shao, Longyi; Niu, Hongya; Yang, Shushen; Shi, Zongbo

DOI:
10.1016/j.envpol.2020.114769

Document Version
Peer reviewed version

Citation for published version (Harvard):
Zhu, Y, Li, W, Lin, Q, Yuan, Q, Liu, L, Zhang, J, Zhang, Y, Shao, L, Niu, H, Yang, S & Shi, Z 2020, 'Iron solubility in fine particles associated with secondary acidic aerosols in east China', *Environmental Pollution*, vol. 264, 114769. https://doi.org/10.1016/j.envpol.2020.114769

Journal Pre-proof

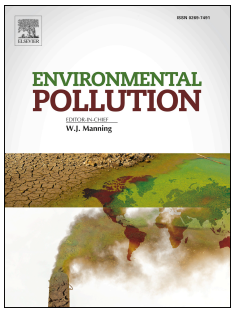

Iron solubility in fine particles associated with secondary acidic aerosols in east China

Yanhong Zhu, Weijun Li, Qiuhan Lin, Qi Yuan, Lei Liu, Jian Zhang, Yinxiao Zhang, Longyi Shao, Hongya Niu, Shushen Yang, Zongbo Shi

PII: S0269-7491(20)32402-7

DOI: https://doi.org/10.1016/j.envpol.2020.114769

Reference: ENPO 114769

To appear in: *Environmental Pollution*

Received Date: 3 April 2020

Revised Date: 4 May 2020

Accepted Date: 6 May 2020

Please cite this article as: Zhu, Y., Li, W., Lin, Q., Yuan, Q., Liu, L., Zhang, J., Zhang, Y., Shao, L., Niu, H., Yang, S., Shi, Z., Iron solubility in fine particles associated with secondary acidic aerosols in east China, *Environmental Pollution* (2020), doi: https://doi.org/10.1016/j.envpol.2020.114769.

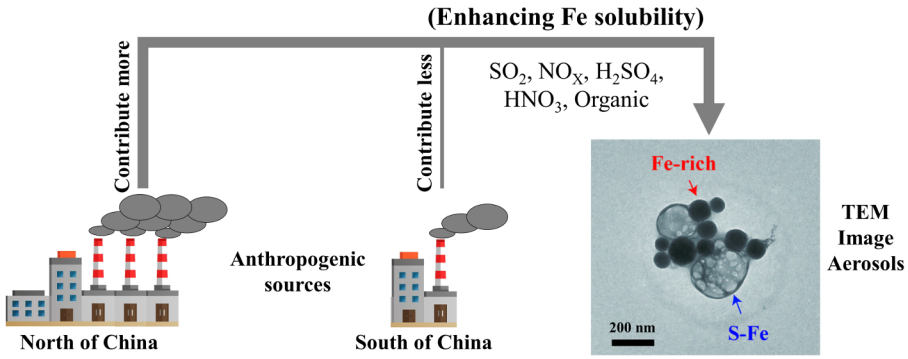

Iron solubility in fine particles associated with secondary acidic aerosols in East China

Yanhong Zhu[a], Weijun Li[a], Qiuhan Lin[a], Qi Yuan[a], Lei Liu[a], Jian Zhang[a], Yinxiao Zhang[a], Longyi Shao[b], Hongya Niu[c], Shushen Yang[d], Zongbo Shi[e]

[a] Department of Atmospheric Sciences, School of Earth Sciences, Zhejiang University, Hangzhou 310027, Zhejiang, China

[b] State Key Laboratory of Coal Resources and Safe Mining, China University of Mining and Technology, Beijing, 100086, China

[c] Key Laboratory of Resource Exploration Research of Hebei Province, Hebei University of Engineering, Handan 056038, China

[d] School of Energy and Environment, Zhongyuan University of Technology, Zhengzhou 450007, China

[e] School of Geography, Earth and Environmental Sciences, University of Birmingham, Birmingham, B15 2TT, UK

*Corresponding author. Email: liweijun@zju.edu.cn

Abstract

Soluble iron (Fe_S) in aerosols contributes to free oxygen radical generation with implications for human health, and potentially catalyzes sulfur dioxide oxidation. It is also an important external source of micronutrients for ocean ecosystems. However, factors controlling Fe_S concentration and its contribution to total iron (Fe_T) in aerosols remain poorly understand. Here, Fe_S and Fe_T in $PM_{2.5}$ was studied at four urban sites in eastern China from 21 to 31 December 2017. Average Fe_T (869-1490 ng m^{-3}) and Fe_S (24-68 ng m^{-3}) concentrations were higher in northern than southern China cities, but Fe solubility (%Fe_S, 2.7-5.0%) showed no spatial pattern. Correlation analyses suggested %Fe_S was strongly correlated with Fe_S and $PM_{2.5}$ instead of Fe_T concentrations. Individual particle observations confirmed that more than 65% of nano-sized Fe-containing particles were internally mixed with sulfates and nitrates. Furthermore, there was a high correlation between sulfates or nitrates/Fe_T molar ratio and %Fe_S. We also found that the sulfates/nitrates had weaker effects on %Fe_S at RH < 50% than at RH > 50%, suggesting RH as indirect factor can influence %Fe_S in $PM_{2.5}$. These results suggest an important role of chemical processing in enhancing %Fe_S in the polluted atmosphere.

Capsule abstract: Iron solubility related to sulfate and nitrate in fine particles in polluted ambient air.

Keywords: Polluted air; Bulk aerosol analysis; Individual particles analysis; Fe solubility; Atmospheric acidification processing

1. Introduction

Iron (Fe) as an important aerosol component is an essential external source for phytoplankton growth in large parts of the remote oceans; it indirectly modulates CO_2 sequestration, and it thus has feedback effects on the global carbon cycle, and climate (Martin and Fitzwater, 1988; De Baar et al., 1995; Jickells et al., 2005; Tagliabue et al., 2017; Matsui et al., 2018). Fe-containing fine particles can adversely affect human health via reactive oxygen species (ROS) formation (Smith and Aust, 1997; Park et al., 2006; Abbaspour et al., 2014). In addition, Fe in aerosol particles or cloud droplets can convert S(IV) to S(VI) by catalytic oxidation, which is a substantial pathway for atmospheric sulfate production (Alexander et al., 2009). These roles of Fe largely depend on the fractional solubility of aerosol Fe (Shi et al., 2012), thus, crucial factors and mechanisms that influence aerosol Fe solubility (%Fe_S) (the concentration ratio of soluble Fe (Fe_S) and total Fe (Fe_T)) need to be better understood.

Fe has natural (e.g., desert dust and soil dust) and anthropogenic (e.g., fossil fuel combustion and steel industrial activities) sources (Mahowald et al., 2005; Jickells et al., 2005; Sedwick et al., 2007). Different sources have different %Fe_S, spanning three orders of magnitude (0.04-81%) (Schroth et al., 2009). Natural emissions are the major sources for Fe_T with a contribution of 70-80% in global air (Jickells et al., 2005), while their %Fe_S is less than 1% (Schroth et al., 2009). Although the contribution of anthropogenic sources to Fe_T is small compared with that from natural sources, their contribution to %Fe_S is much higher (0.06-81%) (Schroth et al., 2009; Oakes et al., 2012). The anthropogenic Fe emissions are strongly associated with anthropogenic combustion sources in regions afflicted with elevated air pollution levels (Guieu et al., 2005; Lough et al., 2005; Sedwick et al., 2007; Zhang et al., 2019). Therefore, it is important to understand %Fe_S in continental air polluted by various anthropogenic sources.

Chemical processing of aerosols during transport and aging in the atmosphere has been hypothesized to influence %Fe_S (Shi et al., 2011; Ito, 2015; Shi et al., 2015; Lin et al., 2019; Xie et al., 2020). Aerosol acidification involving anthropogenic pollutants was thought to be an important hypothesis: acids produced from anthropogenic

pollutants can dissolve aerosol Fe, thus increasing %Fe_S (Meskhidze et al., 2003; Rubasinghege et al., 2010; Zhang et al., 2018). Several studies have estimated aerosol acidity during air polluted periods, but the results differ widely, pH ranging from close to 2 (highly acidic) to about 7 (neutral) in North China based on the chemical modelling calculations (Cheng et al., 2016; Wang et al., 2016; Shi et al., 2017; Guo et al., 2017; He et al., 2018). Such a large pH discrepancy is still under debate because no direct method has been used to measure pH value of individual particles until now. As we know, Fe oxides can be dissolved into Fe_S in aerosol particles under pH < 4 (Shi et al., 2012). Recently, Li et al. (2017) confirmed at the first time that the Fe_S can dissolve from Fe oxides mixed in acidic sulfate particles over East China Sea using transmission electron microscopy (TEM) and nanoscale secondary ion mass spectrometry (NanoSIMS) analysis methods. As this way, if the detailed information of Fe_S can be obtained from bulk aerosol samples, we can provide direct evidence for the fine particles are acidic in bulk sample level. Therefore, understanding mass concentrations of Fe_T and Fe_S as well as the corresponding %Fe_S can be one direct evidence to show aerosol acidity.

In this study, we collected $PM_{2.5}$ and individual particle samples at four urban sites of East China, and combined bulk aerosol and individual particle chemical analysis techniques to investigate: (1) the concentrations of Fe_T, Fe_S, and corresponding %Fe_S; (2) factors influencing %Fe_S, including Fe_S concentration, $PM_{2.5}$ concentration, Fe_T concentration, atmospheric acidification processing, mixing state of Fe-containing particles, and relative humidity (RH).

2. Experimental methods

2.1. Sampling site

Four urban areas were selected to represent typical urban environments: Beijing, Handan, and Zhengzhou in the North China Plain (NCP), and Hangzhou in the Yangtze River Delta (YRD) of southern China (Fig. 1). A population in 2018 is about 21.5, 9.5, 10.1, and 9.8 million in Beijing, Handan, Zhengzhou, and Hangzhou city. The sampling sites in Beijing, Handan, Zhengzhou, and Hangzhou were located in China University of Mining and Technology (Beijing) (CUMTB), Hebei University of

Engineering (HUE), Zhongyuan University of Technology (ZUT), and Zhejiang University (ZU), respectively. The sampling instruments at each sampling site were installed on the rooftop of an academic building with a height of about 15 m above the ground. The surrounding environments of CUMTB, HUE, ZUT, and ZU are similar. They are all situated in the center of the corresponding city, and surrounded by intensive university and residential buildings, business offices and urban streets.

Beijing, the capital of China, is the national center for politics and culture. As a megacity, Beijing mainly suffers from vehicular exhaust pollution. Emissions in Beijing's neighboring regions also significantly influence its air quality due to long-range transport of air pollutants. Zhang et al. (2016) suggested that the regional transport of pollutants contributed 28-36% of $PM_{2.5}$ in Beijing. The annual average concentration of $PM_{2.5}$ was 51 μg m^{-3} in 2018 (source from 2018 Beijing State of Ecological Environment Bulletin), which exceeded the national standard (35 μg m^{-3}) of China.

Handan in northern China is a heavy-industry city with principle industries for steel, coal, cement, coke and electric power generation, whose contribution to Handan GDP has now reached as high as 45% (Handan Statistical Yearbook, 2018). This high energy consumption has resulted in copious emissions of air pollutants. Handan city is among the most polluted cities in China with the annual average $PM_{2.5}$ concentration in 2018 at 69 μg m^{-3} (source from 2018 Hebei Province Ecology and Environment Condition Statement).

Zhengzhou in central China is a coal-driven energy consumption city, with coal burning accounting for about 70% of energy consumption (Jiang et al., 2017). As a hub of the country's major railway, motorway and aviation transportation, Zhengzhou suffers from serious vehicular exhaust pollution. Zhengzhou is often ranked as among the top ten most polluted cities in China with an annual average $PM_{2.5}$ concentration of 63 μg m^{-3} in 2018 (source from 2018 Zhengzhou Environmental Quality Bulletin).

Hangzhou in southeastern China is the second largest city in the Yangtze River Delta (YRD). As one of the most beautiful cities in China, industrial activities in Hangzhou are minor. Traffic emission is one of the most important sources for

Hangzhou air pollution. In addition, pollutants emitted in northern China or in surrounding regions such as some heavy industries in Ningbo are transported into the city to significantly degrade its air quality. The annual average $PM_{2.5}$ concentration was 40 μg m^{-3} in 2018 (source from 2018 Hangzhou Environmental Status Bulletin).

2.2. Sample collection

$PM_{2.5}$ and individual particle samples were collected at the four sampling sites from 21 to 31 December, 2017, only on days without rain. $PM_{2.5}$ samples were collected on 90 mm diameter quartz filters for 11.5 h (daytime: 08:30-20:00; nighttime: 20:30-08:00 (next day)) using a TH-16A Intelligent $PM_{2.5}$ sampler at a flow rate of 100 L min^{-1} (Wuhan Tianhong Corporation, China). Before and after collection, the flow rate was calibrated. Daytime and nighttime blank samples were collected using the same method, but without pumping. Before sample collection, all quartz filters were baked at 600 °C in a muffle furnace for 4 h to remove any possible contaminants. After baking, the quartz filters were placed in a room with temperature of 20 ± 1 °C and RH of 50 ± 2% for 24 h, then, they were weighed using a Sartorius analytical balance (detection limit 0.001 mg). After sample collection, the loaded filters were similarly conditioned and weighed. Difference value of the two weighed mass divide by sample volume was $PM_{2.5}$ concentration.

Individual particle samples were also collected on copper grids coated with carbon film by a single-stage cascade impactor with a 0.3 mm diameter jet nozzle and a flow of 1.0 L min^{-1}. Individual particle samples were collected four times each day at 8:00, 12:00, 18:00 and 0:00. The sampling duration spanned 30 s to 8 min depending on the $PM_{2.5}$ mass concentration. The collection efficiency of the single-stage cascade impactor is 50% for aerodynamic diameter of 0.1 μm particles and a density of 2 g cm^{-3}. After sampling, the grids were placed in a sealed dry plastic tube and stored at 25°C and 20 ± 3% RH in a desiccator.

Meteorological data were measured and recorded every 5 min by an automated weather instrument (Kestrel 5500, USA).

2.3. Fe extraction procedure

2.3.1 Fe_T fraction

The microwave acid digestion was employed to digest the quartz fiber-filter samples into liquid solution for Fe analysis. Firstly, the digestion vessels were cleaned by ultrasonification with ultra-pure water (18.2 MΩ) for 15 min, then with 5% HNO_3 for 15 min, and finally with ultra-pure water for 15 min. Then, one quarter of the sample filters were placed in the digestion vessel with a mixed-acid solution consisting of 6 ml nitric acid (65%, Merck, Germany), 2 ml hydrogen peroxide (> 8%, Beijing Institute of Chemical Reagents, China) and 0.6 ml hydrofluoric acid (40%, Merck, Germany). After closing the vessels, the samples were digested by a microwave digestion system (MARS 5, CEM Corporation, Matthews, NC, USA) on the basis of a temperature-controlled procedure, increasing to 120 °C in 8 min and holding for 3 min, then increasing to 160 °C in 10 min and holding for 10 min, and finally increasing to 190 °C for 10 min and holding for 55 min. After cooling to room temperature, the digested materials was transferred to cleaned brown PTFE bottles and diluted to 100 ml using ultra-pure water. Three blank filters for each sampling site were treated in the same manner as the samples.

2.3.2 Fe_S fraction

Ultrasonification was used to extract the water-soluble fraction of the samples filters for Fe_S analysis following the procedure described by Kanai et al. (2003). One quarter of the sample filters were placed in clean tubes with 15 ml ultra-pure water. Then, the tubes were placed in an ultrasonic bath in ultra-pure water for 60 min. The water extracts were filtered through a 0.22 μm pore size PTFE (polytetrafluoroethylene) syringe filter into cleaned brown PTFE bottles, and subsequently acidified with ultra-pure concentrated HNO_3 to 0.4% v/v HNO_3. Three blank filters for each sampling site were treated in the same manner as the samples. All solutions were stored at 4 °C until instrumental analysis.

2.4. Analytical procedures of Fe

The concentrations of the total and water-soluble fractions of Fe were determined by inductively coupled plasma mass spectrometry (ICP-MS, Agilent 7500ce). Detailed descriptions of the procedure were given in Pan et al. (2013). Briefly, according to the standard procedures and criteria specified in the manufacturer's

manual, the ICP-MS was optimized daily by a tuning solution containing Li, Y, Tl, Ce and Co. External calibration standards (Agilent Technologies, Environmental Calibration Standard) were employed to quantify the Fe, and an internal standard (containing ^{45}Sc, ^{72}Ge, ^{103}Rh, ^{115}In, ^{159}Tb, ^{175}Lu and ^{209}Bi) was added online during Fe analysis. The two certified materials (soil: GBW07401, fly ash: GBW08401) were digested and analyzed in the same manner as the samples for recovery calculation. The recovery of Fe was greater than 95%. Moreover, no significant Fe was found in the field and reagent blank samples. The detection limits of Fe_T and Fe_S were 0.15 and 2.43 $\mu g\ l^{-1}$, respectively.

2.5. Analysis of water-soluble ions, organic carbon, and elemental carbon

Water-soluble ions were analyzed by ion chromatography (Dionex ICs-90, Dionex Corporation, USA). Detailed descriptions about the analytical method were given in Zhang et al. (2017).

Organic carbon (OC) and elemental carbon (EC) were analyzed by a Sunset Laboratory carbon analyzer with the thermal-optical transmittance method. Organic matter (OM) concentrations were obtained by multiplying the OC concentration by 1.91, as reported in Xing et al. (2013).

2.6. Individual particle analysis

The copper grids were analyzed by a JEOL JEM-2100 transmission electron microscope (TEM) combined with an energy-dispersive X-ray spectrometer (EDS). 1613 particles in Beijing samples, 1667 particles in Handan samples, 1523 particles in Zhengzhou samples and 1833 particles in Hangzhou samples were analyzed by the TEM/EDS at 200 kV. TEM does an excellent job of determining the morphology and mixing state of individual particles; EDS detects the main elements above carbon ($\geq$ 12). Copper was not included in the analyses due to the interferences of the copper TEM grids. EDS collection duration was limited to 15 s to reduce beam damage. Five areas from center to periphery of the grids were chosen for analysis to ensure their representativeness. Equivalent circle diameters (ECDs) of the particles were identified by iTEM software (Olympus Soft Imaging Solutions GmbH, Germany).

3. Results and discussion

3.1. Overview of $PM_{2.5}$ pollution

$PM_{2.5}$ concentrations were 155 ± 60 μg m^{-3} in Beijing, 237 ± 71 μg m^{-3} in Handan, 179 ± 90 μg m^{-3} in Zhengzhou, and 93 ± 18 μg m^{-3} in Hangzhou (Table 1) during 21-31 December, 2017, which were all higher than the national daily $PM_{2.5}$ standard of 75 μg m^{-3}. Even the lowest $PM_{2.5}$ concentrations in Beijing (74 μg m^{-3}), Handan (117 μg m^{-3}), Zhengzhou (51 μg m^{-3}), and Hangzhou (71 μg m^{-3}) were close or higher than 75 μg m^{-3}. The day number that $PM_{2.5}$ concentration exceeded 75 μg m^{-3} to total observation days were 10/12, 13/13, 13/14, and 17/18 in Beijing, Handan, Zhengzhou, and Hangzhou city, respectively. In general, $PM_{2.5}$ concentrations were 1.7-2.6 times higher in Beijing, Handan, and Zhengzhou cities in the NCP than in Hangzhou city in the YRD.

OM was the most abundant chemical component in $PM_{2.5}$ in Beijing, Handan, Zhengzhou and Hangzhou cities with contributions of 40%, 31%, 29%, and 31%, respectively (Fig. S1). The next most abundant components in $PM_{2.5}$ were nitrate (NO_3^-), sulfate (SO_4^{2-}), and ammonium (NH_4^+) with contributions of 13%, 8%, and 7% in Beijing, 14%, 9%, and 7% in Handan, 17%, 8%, and 7% in Zhengzhou, and 20%, 9%, and 8% in Hangzhou.

3.2. Overview of individual particles data

A total of 1613, 1667, 1523, and 1833 individual aerosol particles collected in Beijing, Handan, Zhengzhou, and Hangzhou cities, were analyzed by TEM/EDS (Table S1). Based on elemental composition and morphology of individual particles, the internally mixed sulfate particles (e.g., S-OM, S-rich, S-soot, S-fly ash, and S-Fe) were dominant in all the analyzed particles, which were 68% in Beijing, 62% in Handan, 63% in Zhengzhou, and 73% in Hangzhou (Fig. S2). All internally mixed sulfate particles contain S. Because of the detection limitation of TEM/EDS for ammonium nitrate, the technique could not quantify nitrates in individual particles. However, some studies already confirmed that sulfate particles normally contained secondary nitrates in individual secondary particles in urban air (Li et al. 2016; Riemer et al., 2019).

3.3. Fe solubility

Table 1 presents the concentrations of Fe_T and Fe_S in $PM_{2.5}$ as well as $\%Fe_S$ at the four sites. The average Fe_T concentration was 1490 ± 428 ng m^{-3} in Beijing, 1310 ± 271 ng m^{-3} in Handan, 1132 ± 467 ng m^{-3} in Zhengzhou, and 869 ± 215 ng m^{-3} in Hangzhou during 21-31 December, 2017, accounting for 1.14 ± 0.60%, 0.60 ± 0.21%, 0.90 ± 0.58%, and 0.95 ± 0.31% of $PM_{2.5}$, respectively. The average Fe_S concentration was 68 ± 46 ng m^{-3} in Beijing, 59 ± 33 ng m^{-3} in Handan, 32 ± 20 ng m^{-3} in Zhengzhou, and 24 ± 8.5 ng m^{-3} in Hangzhou (Table 1). Fe_T and Fe_S concentrations in the cities of NCP were 1.3-1.7 and 1.3-2.8 times higher than that in the city of YRD, respectively. Here, we calculated $\%Fe_S$ as Fe_S concentration/Fe_T concentration × 100%. The results showed that the average $\%Fe_S$ was 5.0 ± 3.8% in Beijing, 4.5 ± 2.6% in Handan, 2.7 ± 1.5% in Zhengzhou, and 3.0 ± 1.1% in Hangzhou (Table 1). $\%Fe_S$ in Zhengzhou was lower than that in Hangzhou, although Fe_T and Fe_S concentrations in the former were higher than the latter.

We compared the measurements of Fe_T and $\%Fe_S$ with those in the marine atmosphere. Table 2 shows that Fe_T concentrations (869-1490 ng m^{-3}) in this study are much higher than those in the marine atmosphere, ranging from 28.4 ng m^{-3} over the Pacific Ocean (Buck et al., 2013), 218 ng m^{-3} in the North Atlantic Ocean (Buck et al., 2010), 590 ng m^{-3} at the Bay of Bengal (Srinivas et al., 2012), to 761 ng m^{-3} at the East China Sea (Hsu et al., 2010). In contrast, $\%Fe_S$ (2.7%-5.0%) in this study is 1.2-3.3 times lower than those in the marine atmosphere, ranging from 6.0% in the Bay of Bengal, 7.7% in the East China Sea, 8.1% in the Pacific Ocean, to 9.0% in the North Atlantic Ocean. These results indicate that long-range transport of Fe-containing particles significantly increases the $\%Fe_S$ in fine particles.

3.4. Factors influencing Fe solubility

3.4.1 Correlations between $\%Fe_S$ and $PM_{2.5}$, Fe_S, Fe_T

$\%Fe_S$ had strong correlations with Fe_S at all four urban sites with correlation coefficients of 0.81-0.96 (Fig. 2). $\%Fe_S$ and $PM_{2.5}$ also had high correlations with the correlation coefficients at 0.58-0.93, but $\%Fe_S$ had no obvious correlations with Fe_T except the Hangzhou site. In addition, Figure S3 shows that $\%Fe_S$ generally displays similarly variation trend with $PM_{2.5}$ and Fe_S concentrations, but different from Fe_T.

3.4.2 Potential chemical processing in enhancing Fe solubility

To understand what controled the solubility of Fe, we compared $\%Fe_S$ on non-haze, light haze, intermediate haze and heavy haze days (Fig. S4). Here we defined non-haze days as daily $PM_{2.5}$ concentration ≤ 75 μg m^{-3}, light haze days as $75 < PM_{2.5} \leq 150$ μg m^{-3}, intermediate haze days as $150 < PM_{2.5} \leq 250$ μg m^{-3}, and heavy haze days as > 250 μg m^{-3}. Figure S4 shows that $\%Fe_S$ range from 0.9% to 1.2% (average: 1.0% ± 0.2%) on non-haze days, 1.4% to 6.3% (average: 2.9% ± 1.2%) on light haze days, 1.5% to 10.6% (average: 4.4% ± 2.7%) on intermediate haze days and 3.8% to 11.4% (average: 6.5% ± 2.6%) on heavy haze days. In a word, the $\%Fe_S$ significantly increased from non-haze to heavy haze days at each sampling site. There are two possible reasons to explain the increased $\%Fe_S$ following the heavy haze formation: (1) changes in sources, and (2) chemical processing.

Here we firstly investigated the Fe_T contributions from various primary emissions, which were calculated by Fe_T concentrations dividing particulate matter concentrations in different sources. Secondly, $\%Fe_S$ was investigated from various primary emissions, and calculated by Fe_S concentrations dividing Fe_T concentrations in different sources. Fe_T contribution ranged approximately from 3.7%-11.9% for coal combustion (Desboeufs et al., 2005; Fu et al., 2012), 0.4%-3.3% for biomass burning (Yamasoe etal., 2000; Lee et al., 2005; Fuzzi et al., 2007; Fu et al., 2012), 0.86%-9.3% for oil combustion (Desboeufs et al., 2005; Schroth et al., 2009; Fu et al., 2012), and 3.1%-8.5% for mineral dust (Schroth et al., 2009; Fu et al., 2012; Shi et al., 2011, 2012). $\%Fe_S$ ranged from 0.06%-0.2% for coal combustion (Desboeufs et al., 2005; Oakes et al., 2012), 2%-46% for biomass burning (Guieu et al., 2005; Bowie et al. 2009; Oakes et al., 2012), 35.7%-77% for oil combustion (Desboefus et al. 2005; Schroth et al., 2009; Oakes et al., 2012), and 0.04%-0.54% for mineral dust (Schroth et al., 2009; Oakes et al., 2012; Shi et al., 2012). In addition, our previous study showed that $\%Fe_S$ in smelter particles (e.g., Fe oxides) from industrial emissions was extremely low (Li et al., 2017). For this type of particles, we used 0.1% as a conservative value.

The contributions of coal combustion, biomass burning, oil combustion, mineral

dust, and industrial emission to $PM_{2.5}$ were 16%-57%, 7%-11.2%, 2%-17.1%, 10%-23.1%, and 12%-20% in Beijing (Yu et al., 2013; Zhang et al., 2013; Ma et al., 2017), 22.3%-25.9%, 6.3%-10.6%, 10.2%-12.8%, 9.1%-10.9%, and 16.2%-24.2% in Handan (Wei et al., 2014; Meng et al., 2016; Wang et al., 2015), 14%-23%, 12%-13%, 7%-23%, 8%-26%, and 4%-26% in Zhengzhou (Geng et al., 2013; Wang et al., 2017; Jiang et al., 2018), and 12.8%-16.7%, 4%-14%, 10.2%-22%, 2%-8.2%, and 2%-9% in Hangzhou (Zhen et al., 2010; Liu et al., 2015).

Based on above data, we can know that coal combustion, industry and mineral dust have extremely low $\%Fe_S$ (< 1%). Although biomass burning and oil combustion having high $\%Fe_S$, their Fe_T contribution to fine particles are low. Using the equation of Fe_T content × $PM_{2.5}$ source apportionment data × 100%, we find that the Fe_T contributions of biomass burning and oil combustion are less than 3.0% in $PM_{2.5}$. In a word, even though the solubility in the two sources is high, their contribution to the Fe_S is low due to their small contribution to Fe_T. Therefore, variations in primary emissions alone are not able to explain the enhanced $\%Fe_S$ during the haze days, which suggests that chemical processing is the key reason leading to enhanced $\%Fe_S$ during haze events.

TEM observations further support this argument. We clearly identified abundant fine Fe-containing particles (including Fe-rich and S-Fe particles) in the samples with a size range of 25 nm to 4 μm (Fig. 4). The number contribution of Fe-containing particles to the total analyzed particles was 9.2% in Beijing, 7.7% in Handan, 6.6% in Zhengzhou, and 5.2% in Hangzhou (Table S1). In particular, we found that S-Fe particles (internally mixed with secondary inorganic aerosols) were dominant in Fe-containing particles. S-Fe particles accounted for 77%, 74%, 68% and 85% in all the Fe-containing particles in Beijing, Handan, Zhengzhou, and Hangzhou, respectively (Table S1). TEM/EDS showed that secondary inorganic parts in S-Fe particles more or less contained elemental Fe (Fig. 3). The phenomenon is consistent with the findings of Li et al. (2017).

Size distributions of individual particles in Figure 4 showed that the peaks of Fe-rich particles were at 325 nm, 225 nm, 175 nm, and 175 nm in Beijing, Handan,

Zhengzhou and Hangzhou, while the corresponding internally mixed S-Fe particles had peaks at 625 nm, 575 nm, 625 nm and 625 nm, respectively. Thus, secondary sulfate/nitrate uptake led to an increase in particle size by 48%-72%.

Figure 5 provides further evidence to support the potential role of acidic species in the enhancement of $\%Fe_S$ in $PM_{2.5}$ during haze days. Hsu et al. (2014) have used the molar ratio of acidic components to Fe_T to indicate the influence of aerosol acidification on the $\%Fe_S$. NO_3^-/Fe_T and SO_4^{2-}/Fe_T molar ratios showed high correlations with $\%Fe_S$ at each sampling site ($r > 0.7$). This suggested a potential role of secondary species, such as sulfuric acid in the dissolution of insoluble Fe in fine particles (Fig. 3 and 5).

RH is influential in the formation and phases of SO_4^{2-} and NO_3^- in the polluted air of East China (Sun et al., 2018; Wu et al., 2018; Zhu et al., 2020). As a result, RH should be an impact factor on $\%Fe_S$ by influencing secondary sulfate and nitrate formation. Sun et al. (2018) showed that solid phases particle started to convert to solid-liquid mixed phase particles when RH was > 50% in polluted urban air. Therefore, we assumed RH at 50% as the threshold of wet aerosols. Here, we investigated the combined effects of RH and aerosol acidic species on $\%Fe_S$ (Fig. 6). Hsu et al. (2010) reported that the dissolution of aerosol Fe was enhanced by the presence of acidic constituents. SO_4^{2-} and NO_3^-, as the two major acidic constituents in $PM_{2.5}$, were examined in this study. We used the molar ratio of $[2SO_4^{2-} + NO_3^-]/Fe_T$ to represent the acidification degree. Figure 6 shows that $\%Fe_S$ ranged from 0.7% to 3.8% in four cities at RH < 50%, even samples with a high degree of acidification. However, $\%Fe_S$ ranged from 1.3% to 11.4% at RH > 50% in four cities. Therefore, our results suggested that the sulfates/nitrates had a weaker effect on $\%Fe_S$ at RH < 50% than at RH > 50% at all the sampling sites. Indeed, RH showed high correlations with $\%Fe_S$ in Beijing, Handan, Zhengzhou and Hangzhou, their correlation coefficients ranged from 0.51 to 0.92 (Fig. S5). In a word, RH appears to be an indirect factor influencing the $\%Fe_S$ in fine particles.

4. Conclusions and atmospheric implications

The study suggests that acidic species contribute to the dissolution of Fe in the internally mixed particles collected in the four polluted urban sites. Our individual particle analysis suggests that most of Fe-containing inorganic particles with size less than 1 μm in urban air have undergone acidic processes. A recent study shows that aerosol acidity increases with decreasing particle size generated from the $(NH_4)_2SO_4$-H_2SO_4 solution (Crag et al, 2018). Since most of the Fe-containing particles are small with the peak size of Fe-rich particles of 175 to 325 nm and S-Fe particles of 575 to 625 nm (Fig. 4), these particles may tend to be more acidic, even though the bulk aerosol pH may be higher (Shi et al., 2017; Liu et al., 2017; Song et al., 2018).

The presence of large amount of Fe_S may catalyze the reactions for secondary sulfate formation in polluted air of China. How the Fe_S, as the dominant soluble metal in fine particles, changes the heterogeneous uptake of hydroxyl peroxy radicals (HO_2) on aerosol should be paid more attention in polluted air in East China (Zou et al., 2019). Moreover, large amounts of tiny Fe particles and their associated Fe_S can be inhaled into the respiratory tract, even into lung tissues, and can cause adverse health effects in urban cities through the generation of oxygen free radicals (Gonet and Maher, 2019).

Under prevailing westerly winds in winter, these Fe-containing particles in Beijing, Handan, Zhengzhou and Hangzhou urban areas can be transported into the East China Sea and possibly influence the oceanic ecosystem. Li et al. (2017) collected atmospheric particles during a research cruise over the East China Sea, and found that 14% of all analyzed particles were Fe-containing particles, and among them, 75% were internal mixtures of sulfate coating and Fe inclusions. Takahashi et al. (2013) observed that anthropogenic Fe emitted from megacities in Eastern Asia was the most important contributor to Fe_S in the North Pacific Ocean. Our study shows that these anthropogenic Fe particles have already been partially dissolved into Fe_S in aerosols before leaving the continental air.

Acknowledgments

This work was funded by the National Key R&D Program of China

(2017YFC0212700), National Natural Science Foundation of China (91844301, 41907186), Zhejiang Provincial Natural Science Foundation of China (LZ19D050001), China Postdoctoral Science Foundation (2019M652059). Zongbo Shi acknowledges funding from the UK Natural Environment Research Council (NE/N007190/1 and NE/S006699/1).

References

Abbaspour, N., Hurrell, R., Kelishadi, R., 2014. Review on iron and its importance for human health. J. Res. Med. Sci. 19, 164-174.

Alexander, B., Park, R.J., Jacob, D.J., Gong, S., 2009. Transition metal□catalyzed oxidation of atmospheric sulfur: Global implications for the sulfur budget. J. Geophys. Res-Atmos. 114. https://doi.org/10.1029/2008JD010486.

Bowie, A.R., Lannuzel, D., Remenyi, T.A., Wagener, T., Lam, P.J., Boyd, P.W., Guieu, C., Townsend, A.T., Trull, T.W., 2009. Biogeochemical iron budgets of the Southern Ocean south of Australia: Decoupling of iron and nutrient cycles in the subantarctic zone by the summertime supply. Global Biogeochem. Cy. 23. https://doi:10.1029/2009GB003500.

Buck, C.S., Landing, W.M., Resing, J., 2013. Pacific Ocean aerosols: Deposition and solubility of iron, aluminum, and other trace elements. Mar. Chem. 157, 117-130. https://doi.org/10.1016/j.marchem.2013.09.005.

Buck, C.S., Landing, W.M., Resing, J.A., Measures, C.I., 2010. The solubility and deposition of aerosol Fe and other trace elements in the North Atlantic Ocean: observations from the A16N CLIVAR/CO2 repeat hydrography section. Mar. Chem. 120, 57-70. https://doi.org/10.1016/j.marchem.2008.08.003.

Cheng, Y., Zheng, G., Wei, C., Mu, Q., Zheng, B., Wang, Z., Gao, M., Zhang, Q., He, K., Carmichael, G., 2016. Reactive nitrogen chemistry in aerosol water as a source of sulfate during haze events in China. Sci. Adv. 2, e1601530. https://doi.org/10.1126/sciadv.1601530.

Craig, R.L., Peterson, P.K., Nandy, L., Lei, Z., Hossain, M.A., Camarena, S., Dodson, R.A., Cook, R.D., Dutcher, C.S., Ault, A.P., 2018. Direct determination of aerosol pH: size-resolved measurements of submicrometer and supermicrometer aqueous particles. Anal. Chem. 90, 11232-11239. https://doi.org/10.1021/acs.analchem.8b00586.

De Baar, H.J., De Jong, J.T., Bakker, D.C., Löscher, B.M., Veth, C., Bathmann, U., Smetacek, V., 1995. Importance of iron for plankton blooms and carbon dioxide drawdown in the Southern Ocean. Nature 373, 412. https://doi.org/10.1038/373412a0.

Desboeufs, K., Sofikitis, A., Losno, R., Colin, J., Ausset, P., 2005. Dissolution and solubility of trace metals from natural and anthropogenic aerosol particulate matter. Chemosphere 58, 195-203. https://doi.org/10.1016/j.chemosphere.2004.02.025.

Fu, H., Lin, J., Shang, G., Dong, W., Grassian, V.H., Carmichael, G.R., Li, Y., Chen, J., 2012. Solubility of iron from combustion source particles in acidic media linked to iron speciation. Environ. Sci. Technol. 46, 11119-11127. https://doi.org/10.1021/es302558m.

Fuzzi, S., Decesari, S., Facchini, M.C., Cavalli, F., Emblico, L., Mircea, M., Andreae, M.O., Trebs, I., Hoffer, A., Guyon, P., 2007. Overview of the inorganic and organic composition of size□segregated aerosol in Rondonia, Brazil, from the biomass□burning period to the onset of the wet season. J. Geophys. Res-Atmos. 112. https://doi.org/10.1029/2005JD006741.

Geng, N., Wang, J., Xu, Y., Zhang, W., Chen, C., Zhang, R., 2013. PM2. 5 in an industrial district of Zhengzhou, China: Chemical composition and source apportionment. Particuology 11, 99-109. https://doi.org/10.1016/j.partic.2012.08.004.

Gonet, T., Maher, B.A., 2019. Airborne, Vehicle-Derived Fe-Bearing Nanoparticles in the Urban Environment: A Review. Environ. Sci. Technol. 53, 9970-9991. https://doi.org/10.1021/acs.est.9b01505.

Guieu, C., Bonnet, S., Wagener, T., Loÿe□Pilot, M.D., 2005. Biomass burning as a source of dissolved iron to the open ocean? Geophys. Res. Lett. 32. https://doi.org/10.1029/2005GL022962.

Guo, H., Weber, R.J., Nenes, A., 2017. High levels of ammonia do not raise fine particle pH sufficiently to yield nitrogen oxide-dominated sulfate production. Sci. Rep. 7, 12109. https://doi.org/10.1038/s41598-017-11704-0.

He, P., Alexander, B., Geng, L., Chi, X., Fan, S., Zhan, H., Kang, H., Zheng, G., Cheng, Y., Su, H., 2018. Isotopic constraints on heterogeneous sulfate production in Beijing haze. Atmos. Chem. Phys. 18, 5515-5528. https://doi.org/10.5194/acp-18-5515-2018.

Hsu, S. C., Wong, G. T., Gong, G. C., Shiah, F. K., Huang, Y. T., Kao, S. J., Tsai, F., Lung, S. C. C., Lin, F. J., Lin, I., 2010. Sources, solubility, and dry deposition of aerosol trace elements over the East China Sea. Mar. Chem. 120, 116-127. https://doi.org/10.1016/j.marchem.2008.10.003.

Hsu, S. C., Gong, G. C., Shiah, F. K., Hung, C. C., Kao, S. J., Zhang, R., Chen, W. N., Chen, C. C., Chou, C. C. K., Lin, Y. C., Lin, F. J., and Lin, S. H., 2014. Sources, solubility, and acid processing of aerosol iron and phosphorous over the South China Sea: East Asian dust and pollution outflows vs. Southeast Asian biomass burning. Atmos. Chem. Phys. Discuss. 14, 21433–21472. https://doi.org/10.5194/acpd-14-21433-2014.

Ito, A., 2015. Atmospheric processing of combustion aerosols as a source of bioavailable iron. Environ. Sci. Technol. Lett. 2, 70-75. https://doi.org/10.1021/acs.estlett.5b00007.

Jiang, N., Li, Q., Su, F., Wang, Q., Yu, X., Kang, P., Zhang, R., Tang, X., 2018. Chemical characteristics and source apportionment of PM2.5 between heavily polluted days and other days in Zhengzhou, China. J. Environ. Sci. 66, 188-198. in Chinese. https://doi.org/10.1016/j.jes.2017.05.006.

Jiang, Q., Li, H., Wang, S., Fu, C., 2017. Study on Causes and Countermeasures of Haze in Zhengzhou. Guangzhou Chemical Industry in China, 45(16), 136-137.

Jickells, T., An, Z., Andersen, K.K., Baker, A., Bergametti, G., Brooks, N., Cao, J., Boyd, P., Duce, R., Hunter, K., 2005. Global iron connections between desert dust, ocean biogeochemistry, and climate. Science 308, 67-71. https://doi.org/10.1126/science.1105959.

Kanai, Y., Ohta, A., Kamioka, H., Terashima, S., Imai, N., Matsuhisa, Y., Kanai, M., Shimizu, H., Takahashi, Y., Kai, K., 2003. Variation of concentrations and physicochemical properties of aeolian dust obtained in east China and Japan from 2001 to 2002. Bulletin of the Geological Survey of Japan 54, 251-268.

Lee, S., Baumann, K., Schauer, J.J., Sheesley, R.J., Naeher, L.P., Meinardi, S., Blake, D.R.,

Edgerton, E.S., Russell, A.G., Clements, M., 2005. Gaseous and particulate emissions from prescribed burning in Georgia. Environ. Sci. Technol. 39, 9049-9056. https://doi.org/10.1021/es051583l.

Li, W., Sun, J., Xu, L., Shi, Z., Riemer, N., Sun, Y., Fu, P., Zhang, J., Lin, Y., Wang, X., 2016. A conceptual framework for mixing structures in individual aerosol particles. J. Geophys. Res-Atmos. 121, 13,784-13,798. https://doi.org/10.1002/2016JD025252.

Li, W., Xu, L., Liu, X., Zhang, J., Lin, Y., Yao, X., Gao, H., Zhang, D., Chen, J., Wang, W., 2017. Air pollution–aerosol interactions produce more bioavailable iron for ocean ecosystems. Sci. Adv. 3, e1601749. https://doi.org/10.1126/sciadv.1601749.

Lin, Q., Bi, X., Zhang, G., Yang, Y., Peng, L., Lian, X., Fu, Y., Li, M., Chen, D., Miller, M., 2019. In-cloud formation of secondary species in iron-containing particles. Atmos. Chem. Phys. 19, 1195-1206. https://doi.org/10.5194/acp-19-1195-2019.

Liu, G., Li, J., Wu, D., Xu, H., 2015. Chemical composition and source apportionment of the ambient PM2.5 in Hangzhou, China. Particuology 18, 135-143. https://doi.org/10.1016/j.partic.2014.03.011.

Liu, M., Song, Y., Zhou, T., Xu, Z., Yan, C., Zheng, M., Wu, Z., Hu, M., Wu, Y., Zhu, T., 2017. Fine particle pH during severe haze episodes in northern China. Geophys. Res. Lett. 44, 5213-5221. https://doi.org/10.1002/2017GL073210.

Lough, G.C., Schauer, J.J., Park, J.-S., Shafer, M.M., DeMinter, J.T., Weinstein, J.P., 2005. Emissions of metals associated with motor vehicle roadways. Environ. Sci. Technol. 39, 826-836. https://doi.org/10.1021/es048715f.

Ma, Q., Wu, Y., Tao, J., Xia, Y., Liu, X., Zhang, D., Han, Z., Zhang, X., Zhang, R., 2017. Variations of chemical composition and source apportionment of PM2.5 during winter haze episodes in Beijing. Aerosol Air Qual. Res. 17, 2791-2803. https://doi.org/10.4209/aaqr.2017.10.0366.

Mahowald, N.M., Baker, A.R., Bergametti, G., Brooks, N., Duce, R.A., Jickells, T.D., Kubilay, N., Prospero, J.M., Tegen, I., 2005. Atmospheric global dust cycle and iron inputs to the ocean. Global Biogeochem. Cy. 19. https://doi.org/10.1029/2004GB002402.

Martin, J.H., Fitzwater, S.E., 1988. Iron deficiency limits phytoplankton growth in the north-east Pacific subarctic. Nature 331, 341. https://doi.org/10.1038/331341a0.

Matsui, H., Mahowald, N.M., Moteki, N., Hamilton, D.S., Ohata, S., Yoshida, A., Koike, M., Scanza, R.A., Flanner, M.G., 2018. Anthropogenic combustion iron as a complex climate forcer. Nat. Commun. 9, 1593. https://doi.org/10.1038/s41467-018-03997-0.

Meng, C., Wang, L., Su, J., Yang, J., Wei, Z., Zhang, F., Ma, S., 2016. Chemical compositions and source apportionment of PM2.5 in Handan City, Hebei Province. Environ. Sci. Technol. 39, 57-64. in Chinese.

Meskhidze, N., Chameides, W., Nenes, A., Chen, G., 2003. Iron mobilization in mineral dust: Can anthropogenic SO2 emissions affect ocean productivity? Geophys. Res. Lett. 30. https://doi.org/10.1029/2003GL018035.

Oakes, M., Ingall, E., Lai, B., Shafer, M., Hays, M., Liu, Z., Russell, A., Weber, R., 2012. Iron solubility related to particle sulfur content in source emission and ambient fine particles. Environ. Sci. Technol. 46, 6637-6644. https://doi.org/10.1021/es300701c.

Pan, Y., Wang, Y., Sun, Y., Tian, S., Cheng, M., 2013. Size-resolved aerosol trace elements at a rural mountainous site in Northern China: importance of regional transport. Sci. Total

Environ. 461, 761-771. https://doi.org/10.1016/j.scitotenv.2013.04.065.

Park, S., Nam, H., Chung, N., Park, J.-D., Lim, Y., 2006. The role of iron in reactive oxygen species generation from diesel exhaust particles. Toxicol. in Vitro 20, 851-857. https://doi.org/10.1016/j.tiv.2005.12.004.

Riemer, N., Ault, A., West, M., Craig, R., Curtis, J., 2019. Aerosol Mixing State: Measurements, Modeling, and Impacts. Rev. Geophys. https://doi.org/10.1029/2018RG000615.

Rubasinghege, G., Lentz, R.W., Scherer, M.M., Grassian, V.H., 2010. Simulated atmospheric processing of iron oxyhydroxide minerals at low pH: roles of particle size and acid anion in iron dissolution. P. Nat. Acad. Sci. 107, 6628-6633. https://doi.org/10.1073/pnas.0910809107.

Schroth, A.W., Crusius, J., Sholkovitz, E.R., Bostick, B.C., 2009. Iron solubility driven by speciation in dust sources to the ocean. Nat. Geosci. 2, 337. https://doi.org/10.1038/ngeo501.

Sedwick, P.N., Sholkovitz, E.R., Church, T.M., 2007. Impact of anthropogenic combustion emissions on the fractional solubility of aerosol iron: Evidence from the Sargasso Sea. Geochem. Geophy. Geosy. 8. https://doi.org/10.1029/2007GC001586.

Shi, G., Xu, J., Peng, X., Xiao, Z., Chen, K., Tian, Y., Guan, X., Feng, Y., Yu, H., Nenes, A., 2017. pH of aerosols in a polluted atmosphere: source contributions to highly acidic aerosol. Environ. Sci. Technol. 51, 4289-4296. https://doi.org/10.1021/acs.est.6b05736.

Shi, Z., Krom, M.D., Bonneville, S., Baker, A.R., Bristow, C., Drake, N., Mann, G., Carslaw, K., McQuaid, J.B., Jickells, T., 2011. Influence of chemical weathering and aging of iron oxides on the potential iron solubility of Saharan dust during simulated atmospheric processing. Global Biogeochem. Cy. 25. https://doi.org/10.1021/es504623x.

Shi, Z., Krom, M.D., Bonneville, S., Benning, L.G., 2015. Atmospheric Processing Outside Clouds Increases Soluble Iron in Mineral Dust. Environ. Sci. Technol. 49, 1472-1477. https://doi.org/10.1016/j.aeolia.2012.03.001.

Shi, Z., Krom, M.D., Jickells, T.D., Bonneville, S., Carslaw, K.S., Mihalopoulos, N., Baker, A.R., Benning, L.G., 2012. Impacts on iron solubility in the mineral dust by processes in the source region and the atmosphere: A review. Aeolian Res. 5, 21-42. https://doi.org/10.1029/2010GB003837.

Smith, K.R., Aust, A.E., 1997. Mobilization of Iron from Urban Particulates Leads to Generation of Reactive Oxygen Species in Vitro and Induction of Ferritin Synthesis in Human Lung Epithelial Cells. Chem. Res. Toxicol. 10, 828-834. https://doi.org/10.1021/tx960164m.

Song, S., Gao, M., Xu, W., Shao, J., Shi, G., Wang, S., Wang, Y., Sun, Y., McElroy, M.B., 2018. Fine-particle pH for Beijing winter haze as inferred from different thermodynamic equilibrium models. Atmos. Chem. Phys. 18, 7423-7438. https://doi.org/10.5194/acp-18-7423-2018.

Srinivas, B., Sarin, M.M., Kumar, A., 2012. Impact of anthropogenic sources on aerosol iron solubility over the Bay of Bengal and the Arabian Sea. Biogeochemistry 110, 257-268. https://doi.org/10.1007/s10533-011-9680-1.

Sun, J., Liu, L., Xu, L., Wang, Y., Wu, Z., Hu, M., Shi, Z., Li, Y., Zhang, X., Chen, J., Li, W., 2018. Key Role of Nitrate in Phase Transitions of Urban Particles: Implications of Important Reactive Surfaces for Secondary Aerosol Formation. J. Geophys. Res-Atmos. 123, 1234-1243. https://doi.org/10.1002/2017JD027264.

Tagliabue, A., Bowie, A.R., Boyd, P.W., Buck, K.N., Johnson, K.S., Saito, M.A., 2017. The integral role of iron in ocean biogeochemistry. Nature 543, 51-59.

https://doi.org/10.1038/nature21058.

Takahashi, Y., Furukawa, T., Kanai, Y., Uematsu, M., Zheng, G., Marcus, M.A., 2013. Seasonal changes in Fe species and soluble Fe concentration in the atmosphere in the Northwest Pacific region based on the analysis of aerosols collected in Tsukuba, Japan. Atmos. Chem. Phys. 13, 7695-7710. https://doi.org/10.5194/acp-13-7695-2013.

Wang, G., Zhang, R., Gomez, M.E., Yang, L., Zamora, M.L., Hu, M., Lin, Y., Peng, J., Guo, S., Meng, J., 2016. Persistent sulfate formation from London Fog to Chinese haze. P. Nat. Acad. Sci. 113, 13630-13635. https://doi.org/10.1073/pnas.1616540113.

Wang, L., Wei, Z., Wei, W., Fu, J.S., Meng, C., Ma, S., 2015. Source apportionment of PM2.5 in top polluted cities in Hebei, China using the CMAQ model. Atmos. Environ. 122, 723-736. https://doi.org/10.1016/j.atmosenv.2015.10.041.

Wang, S., Yu, S., Li, P., Wang, L., Mehmood, K., Liu, W., Yan, R., Zheng, X., 2017. A study of characteristics and origins of haze pollution in Zhengzhou, China, based on observations and hybrid receptor models. Aerosol Air Qual. Res. 17, 513-528. https://doi.org/10.4209/aaqr.2016.06.0238.

Wei, Z., Wang, L.T., Chen, M.Z., Zheng, Y., 2014. The 2013 severe haze over the Southern Hebei, China: PM2. 5 composition and source apportionment. Atmos. Pollut. Res. 5, 759-768. https://doi.org/10.5094/APR.2014.085.

Wu, Z., Wang, Y., Tan, T., Zhu, Y., Li, M., Shang, D., Wang, H., Lu, K., Guo, S., Zeng, L., 2018. Aerosol liquid water driven by anthropogenic inorganic salts: Implying its key role in haze formation over the North China Plain. Environ. Sci. Technol. Lett. 5, 160-166. https://doi.org/10.1021/acs.estlett.8b00021.

Xie, T. T., Lu, S. L., Zeng, J. Y., Rao, L. F., Wang, X. Z., Win, M. S., Zhang, D. Z., Lu, H., Liu, X. C., Wang, Q. Y., 2020. Soluble Fe release from iron-bearing clay mineral particles in acid environment and their oxidative potential. Sci. Total Environ. 726, 138650. https://doi.org/10.1016/j.scitotenv.2020.138650.

Xing, L., Fu, T.-M., Cao, J., Lee, S., Wang, G., Ho, K., Cheng, M.-C., You, C.-F., Wang, T., 2013. Seasonal and spatial variability of the OM/OC mass ratios and high regional correlation between oxalic acid and zinc in Chinese urban organic aerosols. Atmos. Chem. Phys. 13, 4307-4318. https://doi.org/10.5194/acp-13-4307-2013.

Yamasoe, M.A., Artaxo, P., Miguel, A.H., Allen, A.G., 2000. Chemical composition of aerosol particles from direct emissions of vegetation fires in the Amazon Basin: water-soluble species and trace elements. Atmos. Environ. 34, 1641-1653.

Yu, L., Wang, G., Zhang, R., Zhang, L., Song, Y., Wu, B., Li, X., An, K., Chu, J., 2013. Characterization and source apportionment of PM2.5 in an urban environment in Beijing. Aerosol Air Qual. Res. 13, 574-583. https://doi.org/10.4209/aaqr.2012.07.0192.

Zhang, C., Ito, A., Shi, Z., Aita, M.N., Yao, X., Chu, Q., Shi, J., Gong, X., Gao, H., 2019. Fertilization of the Northwest Pacific Ocean by East Asia air pollutants. Global Biogeochem. Cy. 33, 690-702. https://doi.org/10.1029/2018GB006146.

Zhang, G., Lin, Q., Peng, L., Yang, Y., Jiang, F., Liu, F., Song, W., Chen, D., Cai, Z., Bi, X., 2018. Oxalate Formation Enhanced by Fe-Containing Particles and Environmental Implications. Environ. Sci. Technol. 53, 1269-1277. https://doi.org/10.1021/acs.est.8b05280.

Zhang, H., Wang, S., Hao, J., Wang, X., Wang, S., Chai, F., Li, M., 2016. Air pollution and control action in Beijing. J. Clean. Prod. 112, 1519-1527.

https://doi.org/10.1016/j.jclepro.2015.04.092.

Zhang, J., Liu, L., Wang, Y., Ren, Y., Wang, X., Shi, Z., Zhang, D., Che, H., Zhao, H., Liu, Y., 2017. Chemical composition, source, and process of urban aerosols during winter haze formation in Northeast China. Environ. Pollut. 231, 357-366. https://doi.org/10.1016/j.envpol.2017.07.102.

Zhang, R., Jing, J., Tao, J., Hsu, S. C., Wang, G., Cao, J., Lee, C. S. L., Zhu, L., Chen, Z., Zhao, Y., Shen, Z., 2013. Chemical characterization and source apportionment of PM2.5 in Beijing: seasonal perspective. Atmos. Chem. Phys. 13, 7053–7074. https://doi.org/10.5194/acp-13-7053-2013.

Zhen, B., Yinchang, F., Li, J., Shengmao, H., Wengao, L., 2010. Characterization and Source Apportionment of PM2.5 and PM10 in Hangzhou [J]. Environmental Monitoring in China 2, 44-48. https://doi:10.19316/j.issn.1002-6002.2010.02.012.

Zhu, Y., Tilgner, A., Hoffmann, E.H., Herrmann, H., Kawamura, K., Yang, L., Xue, L., Wang, W., 2020. Multiphase MCM/CAPRAM modeling of formation and processing of secondary aerosol constituents observed at the Mt. Tai summer campaign 2014. Atmos. Chem. Phys. in review. https://doi.org/10.5194/acp-2019-982.

Zou, Q., Song, H., Tang, M. J., Lu, K. D., 2019. Measurements of HO2 uptake coefficient on aqueous (NH4)2SO4 aerosol using aerosol flow tube with LIF system. Chinese Chem. Lett. 30, 2236-2240. https://doi.org/10.1016/j.cclet.2019.07.041.

Table 1

$PM_{2.5}$, Fe_T, and Fe_S concentrations as well as $\%Fe_S$ at the four urban sites from NCP to YRD (the numbers in parentheses were minimum and maximum).

	Beijing	Handan	Zhengzhou	Hangzhou
$PM_{2.5}$ (μg m^{-3})	155 ± 60 (74-270)	237 ± 71 (117-378)	179 ± 90 (51-357)	93 ± 18 (71-156)
Fe_T (ng m^{-3})	1490 ± 428 (971-2601)	1310 ± 271 (977-1996)	1132 ± 467 (342-1945)	869 ± 215 (433-1258)
Fe_S (ng m^{-3})	68 ± 46 (15-148)	59 ± 33 (16-119)	32 ± 20 (2.4-72)	24 ± 8.5 (13-53)
$\%Fe_S$	5.0 ± 3.8 (0.9-11)	4.5 ± 2.6 (0.7-9.6)	2.7 ± 1.5 (0.7-5.6)	3.0 ± 1.1 (1.2-5.5)

Table 2

Total Fe (Fe_T) concentration and Fe solubility ($\%Fe_S$) reported in this study and literature data from ocean sites in the world.

Location	Type	Sampling period	Size	Fe_T, ng m^{-3}	$\%Fe_S$	References
Beijing	Urban	21-31 December 2017	$PM_{2.5}$	1490	5.0	This study
Handan	Urban	21-31 December 2017	$PM_{2.5}$	1310	4.5	This study
Zhengzhou	Urban	21-31 December 2017	$PM_{2.5}$	1132	2.7	This study
Hangzhou	Urban	21-31 December 2017	$PM_{2.5}$	869	3.0	This study
North Atlantic Ocean	Ocean	20 June-7 August 2003	TSP	218	9.0	Buck et al., 2010
Pacific Ocean	Ocean	2004-2006	TSP	28.4	8.1	Buck et al., 2013
Bay of Bengal	Ocean	March-April 2006	TSP	590	6.0	Srinivas et al., 2012
East China Sea	Ocean	Spring 2005- Spring 2007	TSP	761	7.7	Hsu et al., 2010

Figure Captions

Fig. 1. Map showing the locations of Beijing, Handan, Zhengzhou and Hangzhou sampling sites. The map is color-coded by surface elevation heights, which were obtained from SRTM (Shuttle Radar Topography Missionv) data (http://srtm.csi.cgiar.org/srtmdata/).

Fig. 2. Correlations of $\%Fe_S$ and Fe_T (ng m^{-3}) (red), $PM_{2.5}$ (μg m^{-3}) (blue) and Fe_S (ng m^{-3}) (black) at the Beijing (a), Handan (b), Zhengzhou (c) and Hangzhou (d).

Fig. 3. TEM images and EDS of Fe-containing particles in this study: (a) TEM image of Fe-containing particle, (b) EDS of Fe-rich particle, (c) EDS of S-Fe particle.

Fig. 4. Size distributions of Fe-rich particle (blue) and internally mixed S-Fe particle (green) at the four urban sites. The distribution pattern is normalized.

Fig. 5. Correlations between $\%Fe_S$ and NO_3^-/Fe_T (red) and SO_4^{2-}/Fe_T (blue) molar ratio at Beijing (a), Handan (b), Zhengzhou (c) and Hangzhou (d).

Fig. 6. Relationships of $\%Fe_S$ with RH and acidification degree molar ratio $(2SO_4^{2-} + NO_3^-)/Fe_T$ in Beijing (red), Handan (blue), Zhengzhou (green) and Hangzhou (purple).

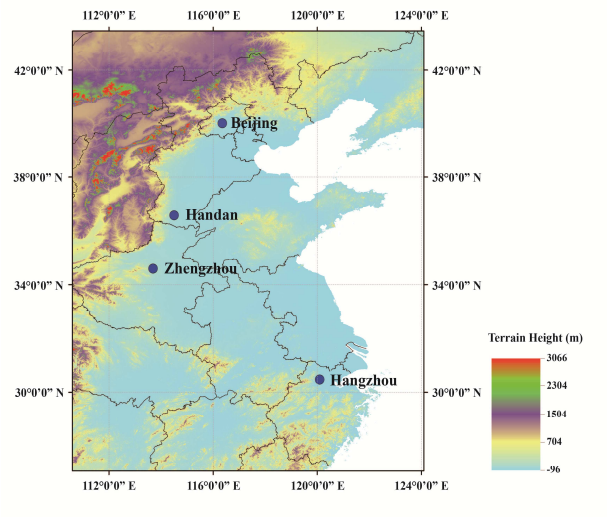

Fig. 1. Map showing the locations of Beijing, Handan, Zhengzhou and Hangzhou sampling sites. The map is color-coded by surface elevation heights, which were obtained from SRTM (Shuttle Radar Topography Missionv) data (http://srtm.csi.cgiar.org/srtmdata/).

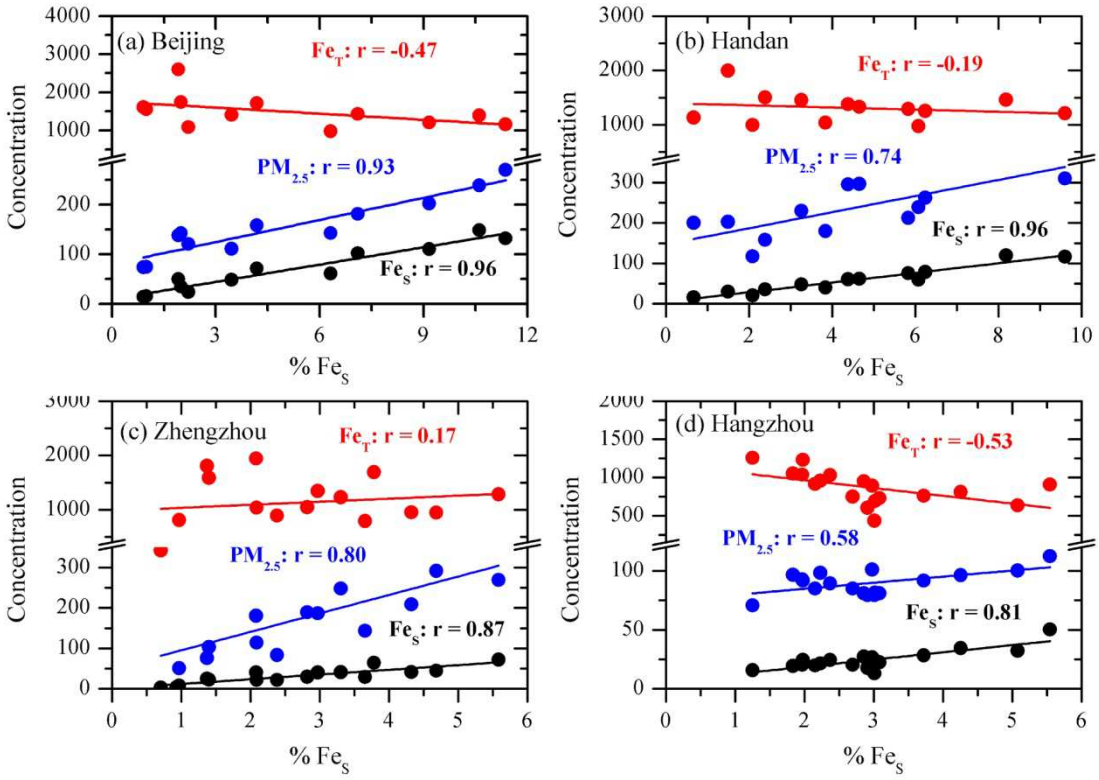

Fig. 2. Correlations of %Fe$_S$ and Fe$_T$ (ng m^{-3}) (red), PM$_{2.5}$ (μg m^{-3}) (blue) and Fe$_S$ (ng m^{-3}) (black) at the Beijing (a), Handan (b), Zhengzhou (c) and Hangzhou (d).

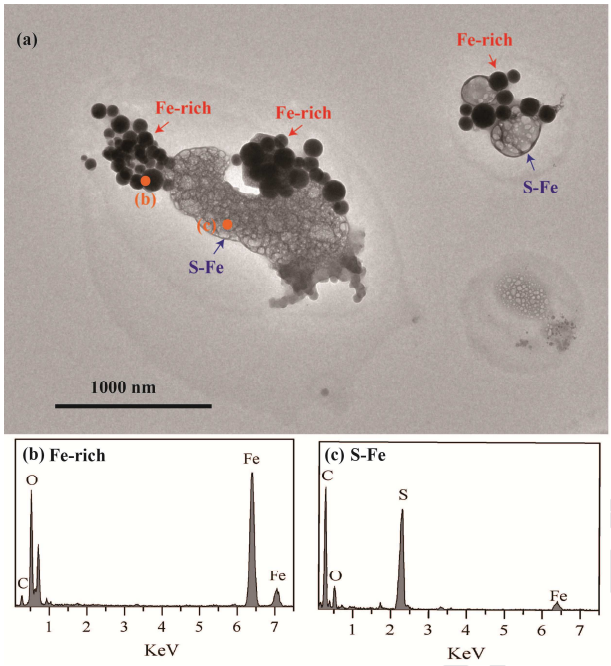

Fig. 3. TEM images and EDS of Fe-containing particles in this study: (a) TEM image of Fe-containing particle, (b) EDS of Fe-rich particle, (c) EDS of S-Fe particle.

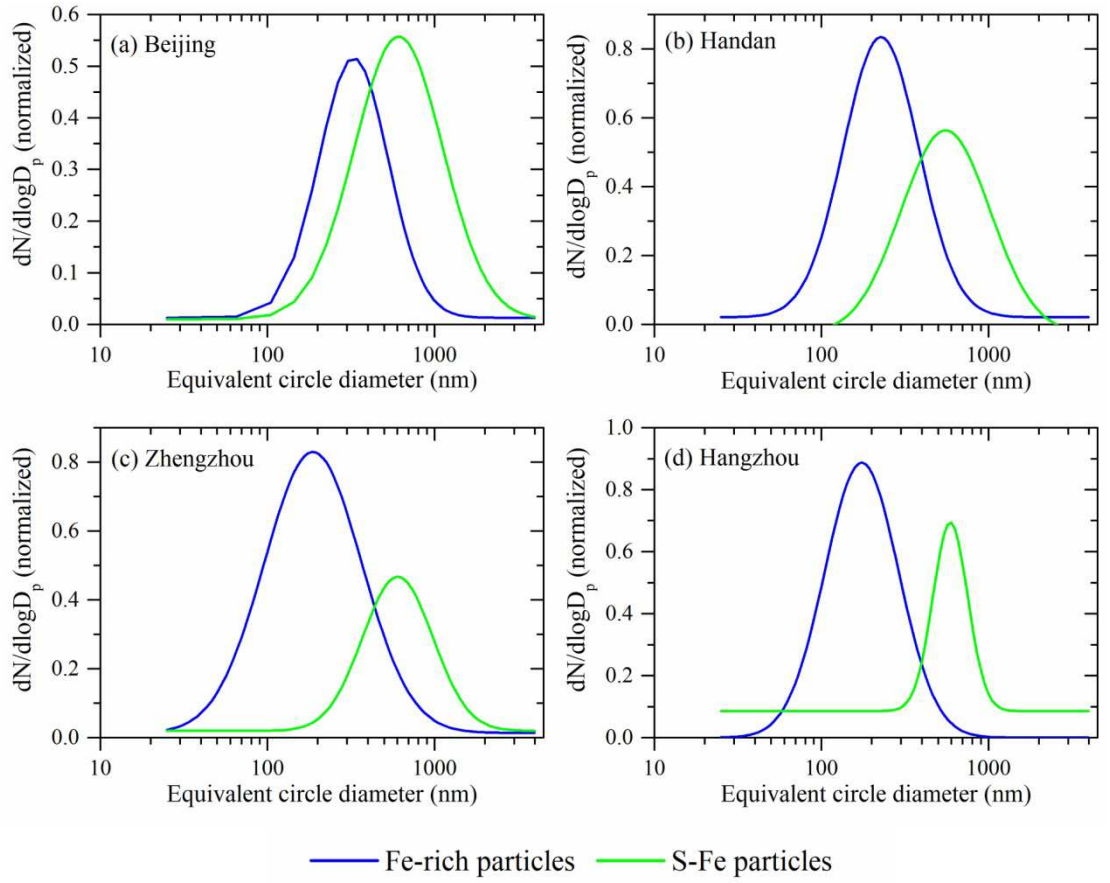

Fig. 4. Size distributions of Fe-rich particle (blue) and internally mixed S-Fe particle (green) at the four urban sites. The distribution pattern is normalized.

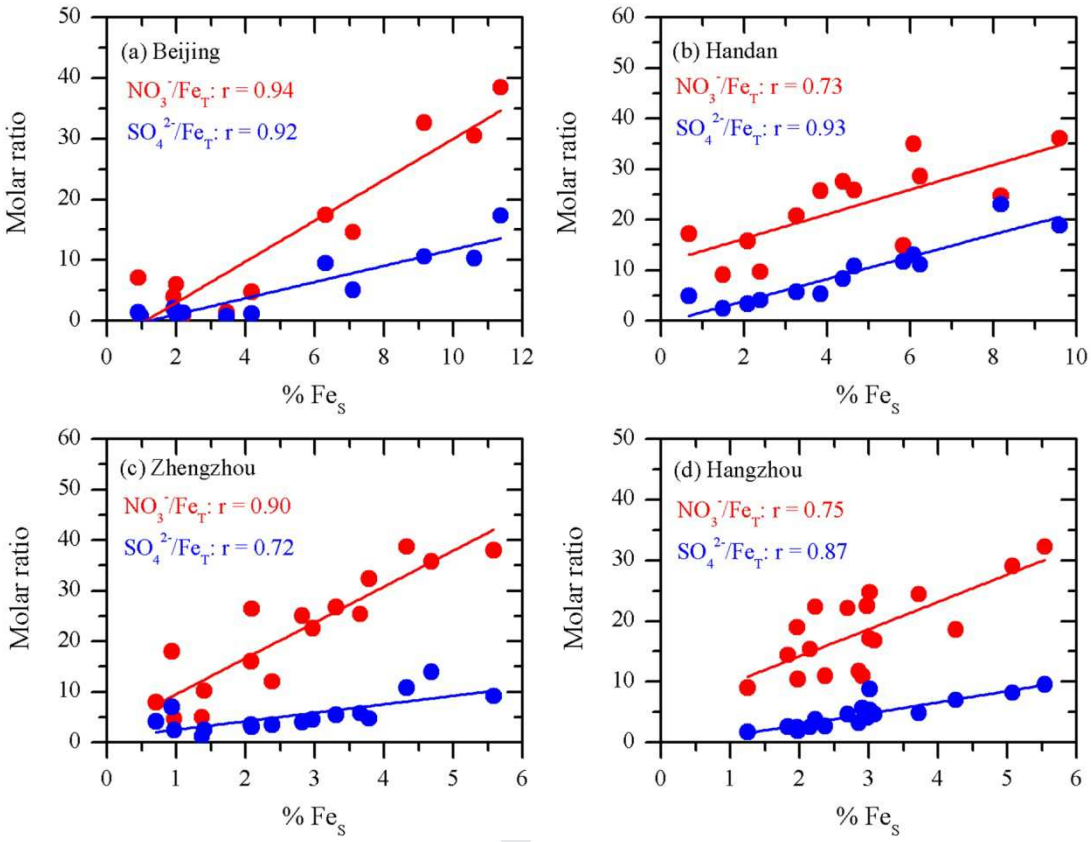

Fig. 5. Correlations between $\%Fe_S$ and NO_3^-/Fe_T (red) and SO_4^{2-}/Fe_T (blue) molar ratio at Beijing (a), Handan (b), Zhengzhou (c) and Hangzhou (d).

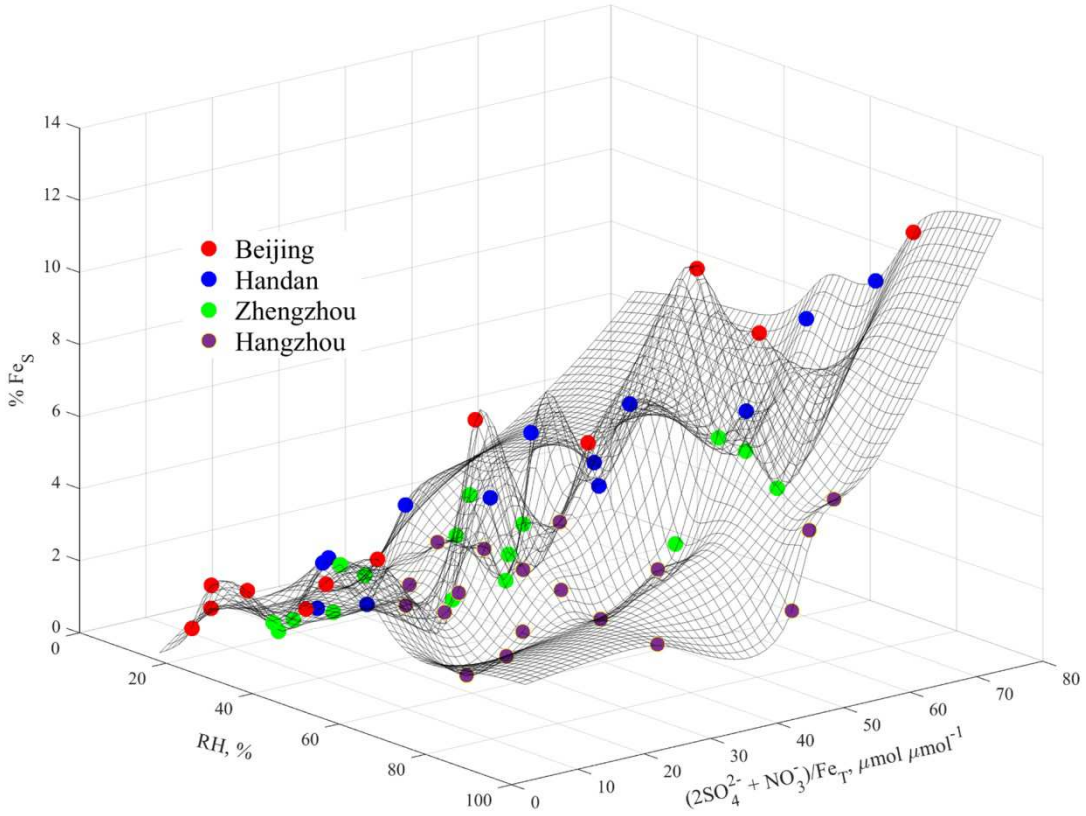

Fig. 6. Relationships of $\%Fe_S$ with RH and acidification degree molar ratio $(2SO_4^{2-} + NO_3^-)/Fe_T$ in Beijing (red), Handan (blue), Zhengzhou (green) and Hangzhou (purple).

Highlights

1. Total iron and soluble iron concentrations as well as iron solubility in polluted air at four urban sites across East China were investigated.

2. A majority of nano-sized Fe-containing particles were internally mixed with sulfates and nitrates.

3. Chemical processing plays an important role in enhancing iron solubility in the polluted atmosphere.

Yanhong Zhu and Weijun Li: Conceptualization, Writing- Original draft preparation. Weijun Li: supervision. Yanhong zhu and Qiuhan Lin: Methodology, Data curation. Lei Liu, Jian Zhang, Qi Yuan, longyi Shao, Hongya Niu, and Shushen Yang: Field Investigation. Zongbo Shi: Writing-Reviewing and Editing,

Declaration of interests

☒ The authors declare that they have no known competing financial interests or personal relationships that could have appeared to influence the work reported in this paper.

☐The authors declare the following financial interests/personal relationships which may be considered as potential competing interests: